MeCP2 deletion impaired layer 2/3-dominant dynamic reorganization of cortical circuit during motor skill learning

Yuanlei Yue[1,2+], Pan Xu[1,2+], Zhichao Liu[3+], Zekai Chen[1], Juntao Su[1], Ai Chen[4], Ryan T. Ash[5], Emre Barut[6], ,Rahul Simha[7], Stelios Smirnakis[8], Chen Zeng[3], Hui Lu[1,2*]

[1]GW Institute for Neuroscience, The George Washington University, Washington, DC 20037, USA

[2]Department of Pharmacology and Physiology, School of Medicine and Health Sciences, The George Washington University, Washington, DC 20037, USA

[3]Department of Physics, Columbia College of Art and Sciences, The George Washington University, Washington, DC 20037, USA

[4]Department of Pediatrics, Affiliated Hospital of Southwest Medical University, Luzhou, Sichuan 646000, China

[4]Department of Psychiatry, Stanford University, Palo Alto, CA 94305, USA

[5]Department of Neurology, Brigham and Women's Hospital, Jamaica Plain VA Hospital, Harvard Medical School, Boston, MA 02115, USA

[6]Department of Statistics, Columbia College of Art and Sciences, The George Washington University, Washington, DC 20037, USA

[7]Department of Computer Science, School of Engineering and Applied Science, The George Washington University, Washington, DC 20037, USA

[8]Department of Neurology, Brigham and Women's Hospital and Jamaica Plain Veterans Administration Hospital, Harvard Medical School, Boston, MA 02115

*Correspondence to: huilu@email.gwu.edu

[+] These authors contributed equally to this work.

Abstract:

Motor cortex displays remarkable plasticity during motor learning. However, it remains largely unknown how the highly dynamic motor cortical circuit reorganizes during *reward-independent* procedural learning at the populational level. Machine learning-based analysis of the neuronal events recorded with in vivo two-photon calcium imaging revealed procedural learning-induced circuit reorganization in superficial but not deep layers of the motor cortex while mice learned to run on a speed-controlled treadmill. Mice lacking Methyl-CpG-binding protein (MeCP2), an animal model for Rett Syndrome, exhibited impaired both procedural learning and dynamic circuit reorganization in layer 2/3, but not layer 5a. These results identify potential circuit mechanisms underlying motor skill learning disability caused by MeCP2 deletion and provide insight in developing therapies for Rett syndrome.

Introduction

Intact motor cortex is shown to be required for skilled movements (Ramanathan et al., 2006). Cortical plasticity underlying motor skill acquisition has been under intense examination with multielectrode array recordings or 2-photon imaging over the primary motor cortex of head-fixed rodents (Chen et al., 2015; Cichon and Gan, 2015; Costa et al., 2004; Komiyama et al., 2010; Masamizu et al., 2014; Peters et al., 2014; Xu et al., 2009; Yang et al., 2009; Yin et al., 2009). These studies showed that, after training in days to weeks, head-fixed rodents can acquire skills to improve their performance in tasks, such as reaching tasks involving grabbing a pellet of food through a small slot, licking tasks involving licking in response to sensory cues, and lever manipulation tasks. These studies demonstrated that plastic changes in the functional topography of the primary motor cortex accompany motor skill acquisition. However, due to the limitations of classical analytic approaches, current available dynamical models of motor cortical function only provide temporal evolution of neural activity during motor skill acquisition and remain agnostic as to how these patterns are organized spatially within the circuit and whether this organization serves a useful role within the neural circuitry in generating skill-related activity patterns. Taking advantage of recent developments in machine learning, we analyzed the neural population coding for motor skill learning and the circuit mechanisms underlying motor learning deficits in mice harboring a genomic deletion of Methyl-CpG-binding protein (MeCP2) -- a model for the neurological disorder Rett syndrome (Amir et al., 1999).

Results

Reward pathways are known to be significantly impacted by MeCP2 deletion (Samaco et al., 2009). Therefore to exclude deficits in reward-related signaling as a mechanism for any observed changes in learning-associated plasticity, we trained 8 week-old head-fixed male mice to locomote on a computerized wheel-treadmill, a *reward-independent* motor learning task. We

simultaneously recorded the neuronal activities of the pyramidal neurons in both layer (L) 2/3 and 5a of the right M1 area and the forelimb kinematics of the mice while they adapted to induced running on the treadmill at different speeds, starting at rest and increasing by 15 mm/sec every 120 seconds up to 60 mm/sec, followed by a 120 sec rest period, then starting at 60 mm/sec and decreasing by 15 mm/sec every 120 seconds down to 0 mm/sec (five total speeds: 0, 15, 30, 45, 60 mm/sec, two 120-second blocks per speed). This experiment was performed daily for 14 consecutive days (Fig. 1A). This type of motor skill learning belongs to procedural learning – a process showing improvement in speed, accuracy, or consistency of a movement with training (Papale and Hooks, 2018). Wild type (WT) mice actively moved their paws in response to the moving treadmill, whereas the paws of *Mecp2-null* (Null) mice often had difficulty in following the treadmill (indicated by the red arrows in Fig. 1, B and C). Paw locations were tracked by a deep learning-based method, LEAP (LEAP Estimates Animal Pose) modified from that documented in a recent report (Pereira et al., 2019) (Fig. S1, A and B). After 7 days (early learning phase), WT mice significantly improved the consistency of paw movement, reflected by stabilized range and decreased kurtosis (a measure of the "tailedness" of the probability distribution, reflecting how often the paw moved significantly outside of its general path through space during locomotion) and skewness (a measure of symmetry of the paw's locomotor path, with positive values representing X, negative values representing Y, and 0 being completely symmetric) of the distribution of paw locations on the treadmill (Fig. 1, E to G, Fig. S1C, and Video 1). The paw location distribution of Null mice showed significantly smaller range and less change of kurtosis and skewness than WT littermates. Interestingly, the negative kurtosis seen in the Null paw kinetics was attributable to an abnormal multimodal distribution of paw locations per animal (Fig. 1H); while in WT mice the probability distribution of paw location generally had a single peak (Fig 1 D top panels), in Null mice the probability distribution of paw location had multiple peaks, revealing a prominent irregularity of paw movements not seen in WT - a sign of motor skill learning deficit (video 2). The learning process was similar for slow and fast learning speed (Fig. S1D).

The data shown was for the left paw as the circuit activity in the right M1 area was measured. Two front paws showed similar learning process.

During motor skill learning, we measured the activity of the pyramidal neurons in layer (L) 2/3 (200-250 μm deep) and 5a (450-500 μm deep, confirmed with L5-specific Rbp4-Cre line, Fig. 2A, Fig. S2A) of area M1 which provide immediate primary input to L5b corticospinal neurons projecting to the spinal cord to orchestrate movements (Georgopoulos and Carpenter, 2015; Papale and Hooks, 2018; Shepherd, 2013). The soma size in L5a is evidently larger than that in L2/3 (Fig. S2B). We computed the event rate of the detected neurons and found that pyramidal neurons in L2/3 increased significantly during running compared to rest on average, for both WT and Null mice. In addition, both L2/3 and L5a of Null mice exhibited lower event rate during running, but not at rest (speed 0) (Fig. S3 and Fig. 2B). The differences did not depend on the layer, running speed, or direction of speed change (i.e. increased from the previous block vs. decreased from the previous block, Fig. S4 and S5). The peak event rate in L2/3 of both WT and Null mice appeared in the middle of the first week (early learning phase), while L5a neurons changed their firing rate with smaller range and longer term. Little change of the firing rate of L5a neurons was presented in Null mice (Fig. S4 and S5). Thus, loss of MeCP2 caused hypoactivity in the superficial layers of M1 and impaired event rate plasticity in both L2/3 and 5a.

To crack the neuronal coding for the paw movement, we examined the contribution of each neuron in coding the paw movement on the treadmill by calculating its weight that evaluates how well its neuronal activity correlates with the paw movement. We trained a Random Forest Regressor (100 trees, minimum leaf size 1) with the criterion of Mean Squared Error (MSE) and bootstrap at different speeds. As can be seen, the weight for speed coding in each neuron varied dramatically from day to day for a given neuron, emphasizing the dynamic nature of the circuit (Fig. S6 C). To simplify comparison, we extracted 10 out of ~200 neurons on average in L2/3 of each animal with top weights that can provide over 95% accuracy of speed coding. In Null mice,

over the whole learning period, the weights of the top 10 best encoding neurons are significantly lower than those in WT mice (Fig. S6, D and E), revealing a weakened coding of running speed in Null mice. While following the circuit encoding over multiple days, we found the weight value peaked in the early few days of learning, followed by a rapid decline and reached the plateau in the late learning phase in WT mice (Fig. S6 E and Fig. S6, A and B). The neurons in L5a did not show such robust difference in speed coding (Fig. S6, F and G). These results reflected a process of circuit exploration and reorganization during learning (Peters et al., 2017a). Null mouse failed to exhibit this phenomenon, indicating impaired circuit plasticity caused by MeCP2 deletion.

Similarly to corticospinal neurons (Peters et al., 2017b), motor cortical neurons in the superficial layers were heterogeneously correlated with movement on the treadmill. Some neurons from both layers are more active or inactive during the transition of the running speeds. We named them transition ON or OFF neurons, respectively (Fig. 2C). The rest of the neurons are steadily active regardless of the transition (OTHER type). These ON and OFF neurons existed in both WT and Null mice. The fraction of each type of neurons showed no difference between the two groups of mice across 14 days (Fig. 2D), whereas the event rate in response to running at high speed was always lower in either type of Null neurons (Fig. 2E). Thus, loss of MeCP2 impacted the excitability, rather than the functionality, of these pyramidal neurons in the superficial layers of the motor cortex. When monitoring the activity of one neuron throughout multiple days, we found the characteristics with regards to the speed transition varied across different days (Fig. 2, F and G), but with similar probability between WT and Null groups (Fig. 2H), revealing a highly dynamic and heterogeneous neuronal ensemble involved in the motor skill learning.

The dynamism of the activity within individual neurons promoted us to employ a powerful platform based on machine-learning approaches to investigate how the highly dynamic neural ensemble learned to encode motor skill learning. Given the fact that traditional machine learning models treat each neuron independently and ignore the potential spatial and topological

correlation between neurons, we implemented variational autoencoder (VAE) with the latent embedding dimension of two using an open-source deep learning software Keras (Exxact Corporation, CA) (Fig. S7). The complexity of the auto-encoder, which was determined through the number of hidden layers in the auto-encoder, was adjusted to assure that the latent space encodes the input without any significant loss of information. Hence, it can achieve sufficient dimension reduction. The latent distribution for the imaging movie frames was related to the treadmill speed as shown in Fig. 3A. The L2/3 neural ensemble in the WT mice clearly showed distinct features (separated clustering reflected by decreased overlap ratio between speed 0 and 60 mm/sec) in coding running and rest states with no preference for the running speeds after the early learning phase(Fig. 3 B top row, C and D), while the L5A neural ensemble did not differentiate between speeds (Fig. 3B bottom row). The individual animals in the WT group showed consistent change of the relationship between the overlap ratio (circuit reorganization) and kurtosis (motor skill learning), but not the animals in Null group (Fig. 3E). Null circuits not only failed to show such separation of coding features but also presented larger variation on the radius of the feature distribution across days (Fig. S8), indicating the cluelessness of circuit organization.

Using Principal Components Analysis (PCA) on the neural ensemble composed of the same group of neurons identified via performing global alignment throughout 14 days (Fig. 3F and Fig. S9), we found that the trajectories for running in the WT mice, but not for rest, expanded in early few days and then converged after the early learning phase. This result indicated that the circuit was reorganized during the early phase and stabilized in the late phase of learning. This trend did not occur in the Null mice, illuminating the failure of circuit reorganization in support of the result from VAE analysis (Fig. 3, F and G). In WT mice, such a trend was shown for all running speeds. Thus, the neural circuit may be reorganized to encode the movement that the mouse was trying to adapt during learning. In support of this speculation, we adopted a supervised machine-learning approach to predict the running speeds on a day using the circuit activity from a prior day (Fig. 3H). The stabilized circuit should be able to offer higher prediction accuracy than the non-stabilized circuit. Indeed, the accuracy in

the WT circuit increased gradually and reached a plateau after the early phase, a time course matched well with the alteration of behavior (Fig. 1), event rate (Fig. 2) and circuit dynamics (Fig. 3, A to G), whereas an opposite trend occurred in the Null mice (Fig. 3, I and J). Thus, in association with motor skill learning, the neural circuit in L2/3 of M1 area was reorganized to encode the speed in a pattern that was more robust than that in L5a. This result suggests that L2/3 circuit is more involved in motor skill learning than L5/a, consistent with a previous finding using reward-driven lever pressing skill learning (Peters et al., 2017b).

Discussion

Taken together, our study adopted machine learning-based approaches to reveal that the malleable M1 circuits in different layers responded to procedural learning in a distinct time course and pattern of circuit reorganization. The plasticity of neuronal activity and circuit organization occurred faster and stronger in L2/3 compared to L5a, suggesting that these two layers might play different roles in establishing learned circuit dynamics to flow into the downstream corticospinal system, as described in a previous study using reward-driven motor skill learning (Masamizu et al., 2014; Peters et al., 2017b). The machine-learning approaches effectively helped to generate crucial insight into how the highly dynamic motor circuit encodes complex locomotion behavior and how, when impaired, motor dysfunction develops. It offered a novel insight on the impairment of motor circuit plasticity in association with motor learning deficit caused by loss of MeCP2. To our knowledge, this circuit-level abnormality is not previously reported in this Rett syndrome mouse model. Further study is needed to tease out the relative contributions to Null mouse motor learning deficit, from dysfunction in sensory processing circuits (as indicated by the slower response in hot plate test (Samaco et al., 2013), abnormal motor/premotor cortical circuit processing (Eyre et al., 1990), or weaker muscle strength (Wu et al., 2016). The minimal abnormalities detected in L5A corticostriatal neurons suggest that corticostriatal circuits may be less affected in Null mice. Together, these results provide insights

into the function of the neural substrates underlying motor learning and an important target for alleviating motor learning deficits in Rett syndrome.

.

Acknowledgements

We would like to thank Dr. Huda Zoghbi at Baylor College of Medicine for providing the MeCP2 mutant mouse line. We thank Hongfei Du and Dr. Emre Barut for help with Matlab and statistics.; **Funding:** This work was supported by funding from the NIH grant 5R00NS089824 and grants from March of Dimes Basil O'Connor Starter Scholar Research Award grant #5-FY18-3 and The George Washington University 2018 Cross-Disciplinary Research Fund to H. L and C.Z; **Author contributions:** Y.Y., P.X., and H.L. designed and performed the experiments. Y.Y., P.X., Z.L., Z.C., J.S., A.C. R.T.A., S.S., C.Z. and H.L. reviewed and interpreted data. Y.Y., Z.L., Z.C., and J.S. performed the data analysis. Y.Y., Z.L., Z.C., J.S., R.T.A., E.B. and H.L. wrote the manuscript with critical input from P.X., A.C., S.S., and C.Z.; **Competing interests:** Authors declare no competing interests; **Data and materials availability:** All data and codes in the main text or the supplementary materials are available upon request.

References

Amir, R.E., Van Den Veyver, I.B., Wan, M., Tran, C.Q., Francke, U., and Zoghbi, H.Y. (1999). Rett syndrome is caused by mutations in X-linked MECP2, encoding methyl- CpG-binding protein 2. Nat. Genet.

Chen, S.X., Kim, A.N., Peters, A.J., and Komiyama, T. (2015). Subtype-specific plasticity of inhibitory circuits in motor cortex during motor learning. Nat. Neurosci.

Cichon, J., and Gan, W.B. (2015). Branch-specific dendritic Ca2+ spikes cause persistent synaptic plasticity. Nature.

Costa, R.M., Cohen, D., and Nicolelis, M.A.L. (2004). Differential corticostriatal plasticity during fast and slow motor skill learning in mice. Curr. Biol.

Eyre, J.A., O'Sullivan, M.C., Ramesh, V., Miller, S., and Kerr, A.M. (1990). Neurophysiological observations on corticospinal projections to the upper limb in subjects with Rett syndrome. J. Neurol. Neurosurg. Psychiatry.

Georgopoulos, A.P., and Carpenter, A.F. (2015). Coding of movements in the motor cortex. Curr. Opin. Neurobiol. *33*, 34–39.

Komiyama, T., Sato, T.R., Connor, D.H.O., Zhang, Y., Huber, D., Hooks, B.M., Gabitto, M., Svoboda, K., O'Connor, D.H., Zhang, Y., et al. (2010). Learning-related fine-scale specificity imaged in motor cortex circuits of behaving mice. Nature *464*, 1182–1186.

Masamizu, Y., Tanaka, Y.R., Tanaka, Y.H., Hira, R., Ohkubo, F., Kitamura, K., Isomura, Y., Okada, T., and Matsuzaki, M. (2014). Two distinct layer-specific dynamics of cortical ensembles during learning of a motor task. Nat. Neurosci.

Papale, A.E., and Hooks, B.M. (2018). Circuit changes in motor cortex during motor skill learning. Neuroscience *368*, 283–297.

Pereira, T.D., Aldarondo, D.E., Willmore, L., Kislin, M., Wang, S.S.H., Murthy, M., and Shaevitz, J.W. (2019). Fast animal pose estimation using deep neural networks. Nat. Methods.

Peters, A.J., Chen, S.X., and Komiyama, T. (2014). Emergence of reproducible spatiotemporal activity during motor learning. Nature *510*, 263–267.

Peters, A.J., Liu, H., and Komiyama, T. (2017a). Learning in the Rodent Motor Cortex. Annu. Rev. Neurosci.

Peters, A.J., Lee, J., Hedrick, N.G., O'neil, K., and Komiyama, T. (2017b). Reorganization of corticospinal output during motor learning. Nat. Neurosci. *20*.

Ramanathan, D., Conner, J.M., and Tuszynski, M.H. (2006). A form of motor cortical plasticity that correlates with recovery of function after brain injury. Proc. Natl. Acad. Sci. U. S. A.

Samaco, R.C., Mandel-Brehm, C., Chao, H.-T., Ward, C.S., Fyffe-Maricich, S.L., Ren, J., Hyland, K., Thaller, C., Maricich, S.M., Humphreys, P., et al. (2009). Loss of MeCP2 in aminergic neurons causes cell-autonomous defects in neurotransmitter synthesis and specific behavioral abnormalities. Proc. Natl. Acad. Sci.

Samaco, R.C., Mcgraw, C.M., Ward, C.S., Sun, Y., Neul, J.L., and Zoghbi, H.Y. (2013). Female Mecp2+/- mice display robust behavioral deficits on two different genetic backgrounds providing a framework for pre-clinical studies. Hum. Mol. Genet. *22*, 96–109.

Shepherd, G.M.G. (2013). Corticostriatal connectivity and its role in disease. Nat. Rev. Neurosci. *14*, 278–291.

Wu, Y., Zhong, W., Cui, N., Johnson, C.M., Xing, H., Zhang, S., and Jiang, C. (2016). Characterization of Rett Syndrome-like phenotypes in Mecp2-knockout rats. J. Neurodev. Disord.

Xu, T., Yu, X., Perlik, A.J., Tobin, W.F., Zweig, J.A., Tennant, K., Jones, T., and Zuo, Y. (2009).

Rapid formation and selective stabilization of synapses for enduring motor memories. Nature.

Yang, G., Pan, F., and Gan, W.B. (2009). Stably maintained dendritic spines are associated with lifelong memories. Nature.

Yin, H.H., Mulcare, S.P., Hilário, M.R.F., Clouse, E., Holloway, T., Davis, M.I., Hansson, A.C., Lovinger, D.M., and Costa, R.M. (2009). Dynamic reorganization of striatal circuits during the acquisition and consolidation of a skill. Nat. Neurosci.

Figure legends

Fig.1. Mice with MeCP2 deletion exhibited motor learning deficit during treadmill running.

(A) A diagram showing head-fixed mouse performing treadmill running task under two-photon microscope. Simultaneous in vivo calcium imaging was performed over layer (L) 2/3 and 5a of the area M1. (B) Frames of paw movie at three representative time points, with paw locations labeled by LEAP method. (C) Sample temporal traces for the locations of the left paw of one WT (black) and one Null (blue) mouse on the treadmill moving at speed 60 during day 14. The paw location at a time point is calculated as the distance between the median paw location and location at that time. Red arrows in B and C indicate the difficult moment for the Null mouse to follow the moving treadmill. (D) Distributions of the paw locations at speed 60 mm/sec during day 1, 7 and 14 of one representative mouse from WT and Null group, respectively. It shows multiple peaks of distribution for the Null mouse. (E-H) Averaged range (E), kurtosis (F), skewness (G), and the number of peaks of paw location distribution across 14 days. Black, WT, n=9 mice; blue, Null, n=9 mice. Error bars represent mean ± SE. * $p < 0.05$; *** $p < 0.001$, linear mixed models for Type III ANOVA test.

Fig. 2. MeCP2 deletion impaired the plasticity of neuronal activity, but not functionality of the M1 pyramid neurons.

(A) Images of pyramidal neurons expressing GCaMP6m in L2/3 (top) and L5a (bottom) of one WT (left) and one Null (right) mouse taken with 25X lens on a two-photon microscope. Next to the images were dF/F (% change in fluorescence intensity, see Methods) calcium traces from the neurons labeled with color-matched circles. (B) Averaged event rate across 14 days for pyramidal neurons in L2/3 (top) and L5a (bottom) at rest (speed 0) and running (speed 60 mm/sec), respectively. (C) Heatmap of neuronal activity around speed transition for transition ON and OFF

neurons in L2/3 (top) and L5a (bottom) from one WT mouse. Arrow indicates the moment when treadmill speed changed from 0 to 60 mm/sec. (D-E) Averaged proportion (D) and event rate (E) of the transition ON and OFF neurons throughout 14 days. WT: n=9; Null: n=8 mice. (F) Response property mapping of 50 neurons from one representative WT mouse across 11 days. WT: N=9 mice; Null: N=8 mice. (G) Top, Images of the same neuron taken at 11 days. Bottom, the trace of fluorescent intensity change ($\Delta F/F$) for 15 seconds before and after speed transition (marked as time zero) in those days. (H) Summary of the probability of response property change of the neurons in WT and Null groups. Red scattered dots represent the value of each animal. WT, N=7; Nul, N=6. Error bars represent mean ± SE. * $p < 0.05$; ** $p < 0.01$, linear mixed models for Type III ANOVA test.

Fig. 3. MeCP2 deletion caused the failure of circuit reorganization associated with motor skill learning.

(A) Two-dimensional spatiotemporal features of the activity pattern in M1 circuit captured in each image during treadmill running at different speeds was extracted by a machine-learning approach VAE and represented in a plot. The activity pattern of 5 sample images with each taken at one speed was represented by the dot indicated by the arrow head. (B) Sample distributions of the spatiotemporal feature extracted for both layers from one WT and one Null mouse by VAE analysis for each frame of in vivo calcium imaging movie at each running speed during day 1, 3 and 7 at speed-up mode. Dots for the frames at the same speed are labeled with the same color. The spatiotemporal features of L2/3 circuit activity in WT mouse at speed 0 displayed apparent separation from those at the running state on day 7, indicated by the red arrow. This separation was absent in L5a circuit and Null circuits. (C) Sample radius of the feature distributions for speed 0 and 60 mm/sec during Day 2 and 14 (see Methods for the radius calculation). (D) Summary of the overlap ratio (top) and radius (bottom) for L2/3 population between the feature distributions of

frames at speed 0 and 60 mm/sec for each day. One dot represents the overlap ratio from one mouse. Solid lines represent the fitting of all data from each group. Black, WT; blue, Null. (E) The relationship between the overlap ratio of circuit feature distribution and kurtosis of motor skill learning from averaged initial day 1-2 and later day 9-10 in each individual animal. Data from the same animal is connected with a solid line. (F) Distribution of the top two principal components (PC1 and PC2) obtained via PCA for the same group of neurons across 11 days. (G) Summary of the averaged distance of 10 PCs between two adjacent days at speed 60 mm/sec (Run) and 0 (rest). Solid line: fitting of mean value; Shadow: S.E.M. (H) Overview of the speed prediction workflow with the deep-learning approach. (I) Sample matrix of prediction accuracy across 11 days from one WT and one Null mouse. (J) Summary of averaged accuracy for 11 days from 7 WT and 5 Null mice. Error bars represent mean ± SE.

Fig. 1

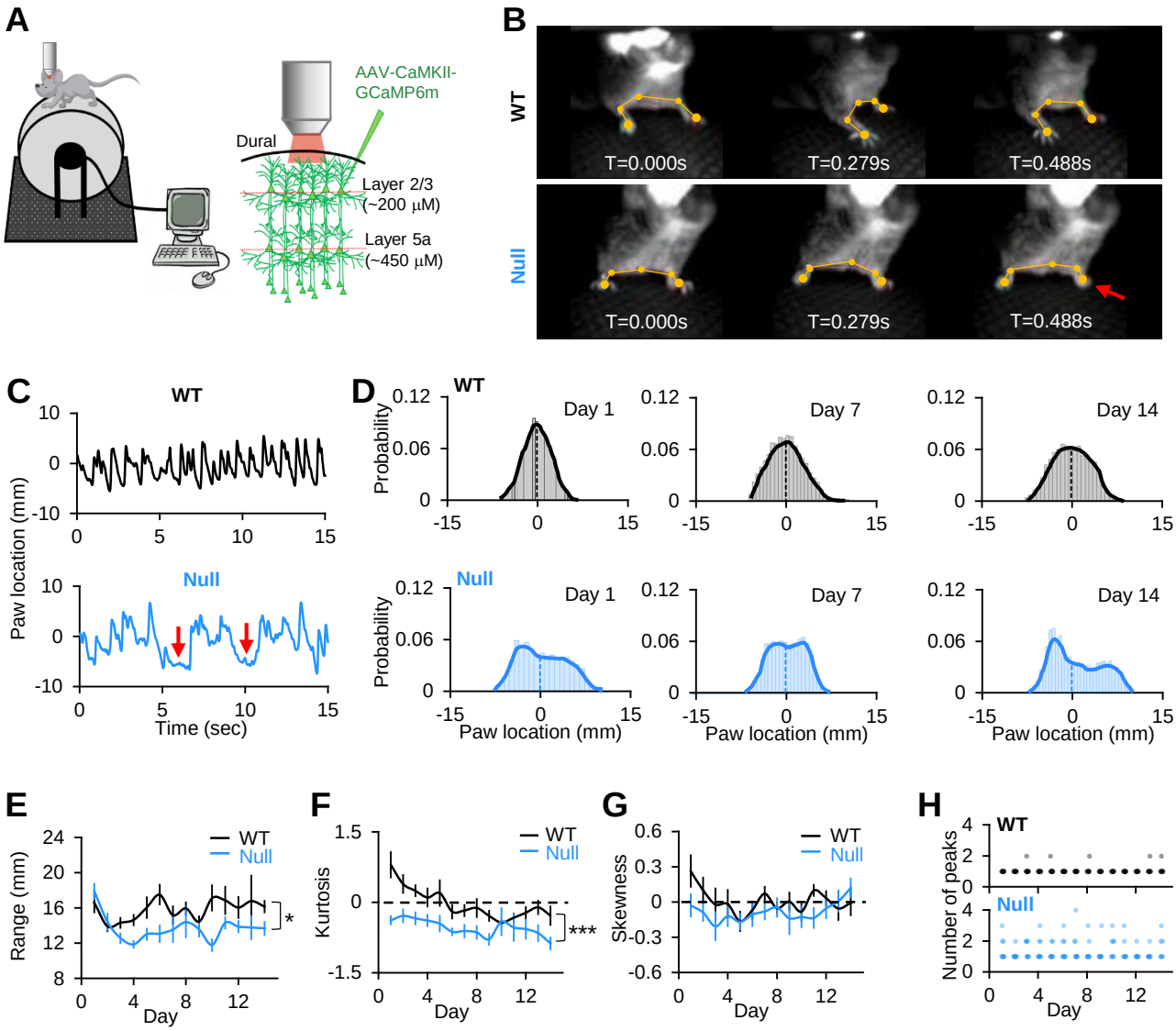
A
AAV-CaMKII-GCaMP6m
Dural
Layer 2/3 (~200 μM)
Layer 5a (~450 μM)
B
WT
Null
T=0.000s
T=0.279s
T=0.488s
C
WT
Null
Paw location (mm)
Time (sec)
D
Day 1
Day 7
Day 14
Probability
Paw location (mm)
E
Range (mm)
Day
WT
Null
F
Kurtosis
Day
G
Skewness
Day
H
Number of peaks
Day

Fig. 2

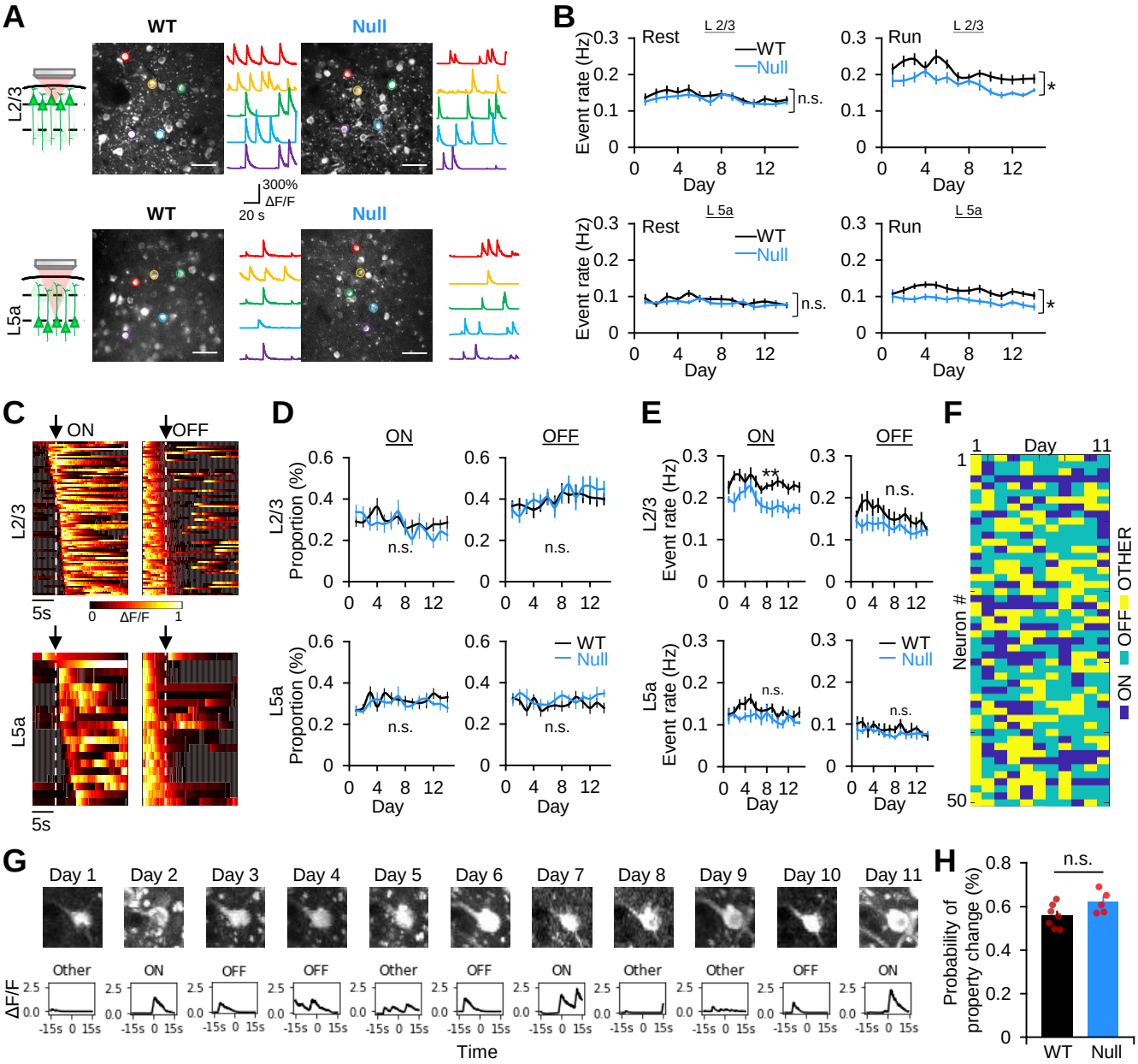
A
WT
Null
L2/3
L5a
300%
ΔF/F
20 s
B
Rest
Run
L 2/3
L 5a
WT
Null
Event rate (Hz)
Day
n.s.
*
C
ON
OFF
L2/3
L5a
5s
ΔF/F
D
Proportion (%)
E
Event rate (Hz)
**
F
Day
Neuron #
OTHER
OFF
ON
G
Day 1
Day 2
Day 3
Day 4
Day 5
Day 6
Day 7
Day 8
Day 9
Day 10
Day 11
Other
ON
OFF
Time
H
Probability of property change (%)
WT
Null

Fig. 3

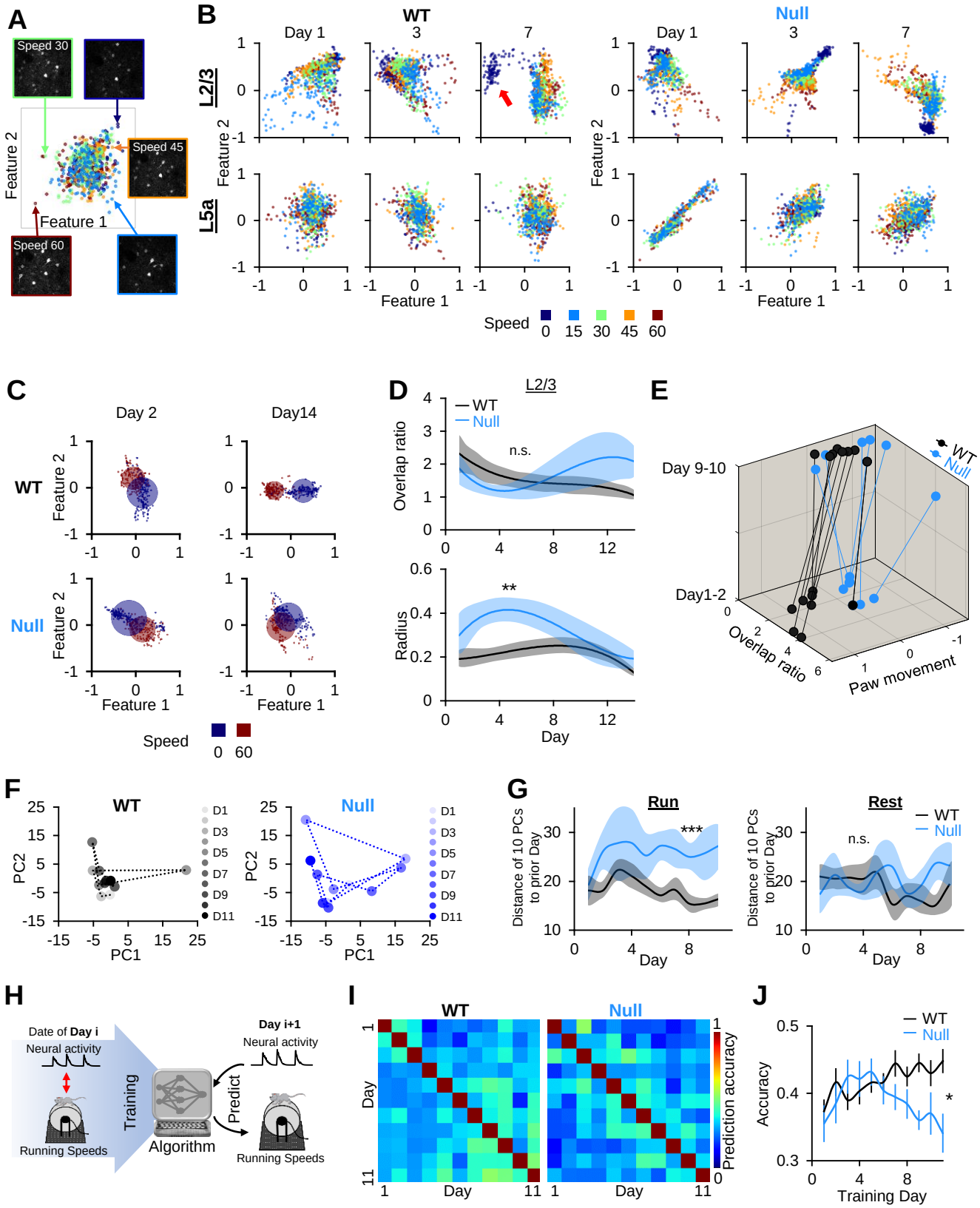
A
Speed 30
Speed 45
Speed 60
Feature 1
Feature 2
B
WT
Null
Day 1
3
7
L2/3
L5a
Feature 2
Feature 1
Speed
0 15 30 45 60
C
Day 2
Day14
WT
Null
Feature 2
Feature 1
Speed
0 60
D
L2/3
WT
Null
Overlap ratio
n.s.
Radius
**
Day
E
Day 9-10
Day1-2
WT
Null
Overlap ratio
Paw movement
F
WT
Null
PC2
PC1
D1
D3
D5
D7
D9
D11
G
Run
Rest
Distance of 10 PCs to prior Day
***
n.s.
WT
Null
Day
H
Date of Day i
Neural activity
Running Speeds
Training
Algorithm
Predict
Day i+1
Neural activity
Running Speeds
I
WT
Null
Day
Prediction accuracy
J
WT
Null
Accuracy
*
Training Day